

Use of Neural Networks in Brain SPECT to Diagnose Alzheimer's Disease

Michael P.A. Page, Robert J. Howard, John T. O'Brien, Muriel S. Buxton-Thomas and Alan D. Pickering
Hellesdon Hospital, Norwich; Department of Psychology, St. George's Hospital Medical School; Section of Old Age Psychiatry, Institute of Psychiatry; and Department of Nuclear Medicine, King's College Hospital, London, United Kingdom

The usefulness of artificial neural networks in the classification of ^{99m}Tc -HMPAO SPECT axial brain scans was investigated in a study group of Alzheimer's disease patients and age-matched normal subjects. **Methods:** The cortical circumferential profiling (CCP) technique was used to extract information regarding patterns of cortical perfusion. Traditional analysis of the CCP data, taken from slices at the level of the basal ganglia, indicated significant perfusion deficits for Alzheimer's disease patients relative to normals, particularly in the left temporo-parietal and left posterior frontal areas of the cortex. The compressed profiles were then used to train a neural-network classifier, the performance of which was compared with that of a number of more traditional statistical (discriminant function) techniques and that of two expert viewers. **Results:** The optimal classification performance of the neural network (ROC area = 0.91) was better than that of the alternative statistical techniques (max. ROC area = 0.85) and that of the expert viewers (max. ROC area = 0.79). **Conclusion:** The CCP produces perfusion profiles which are well suited to automated classification methods, particularly those employing neural networks. The technique has the potential for wide application.

Key Words: Alzheimer's disease; computer-assisted image processing; artificial neural networks; SPECT; technetium-99m-HMPAO

J Nucl Med 1996; 37:195-200

In recent years, artificial neural networks (ANN) have been applied to a broad range of problems in the medical domain (1-9). In this article, we describe their application to the automated diagnosis of Alzheimer's disease from SPECT brain images. In any neural network application, the choice of a format for the input set is of paramount importance: this choice is influenced not only by the likelihood that a given input format will aid the network in performing the required task, but also by computational tractability of the network implied by that format. Such restraints suggest the preprocessing of images so as to extract from each a pattern, or profile, of relatively low dimension, which nonetheless contains sufficient information to enable diagnosis to be learned and performed. It is, of course, preferable that the extraction of this profile should not itself be computationally expensive and/or time-consuming in terms of operator intervention.

Previous work with SPECT perfusion images of Alzheimer's disease patients has suggested that the pattern of cortical perfusion deficits is strongly indicative of the disease (10-14). We now describe a particular technique for extracting a low-dimensional profile of cortical perfusion from a given axial brain SPECT image before detailing the means by which such profiles can be used for automated diagnosis.

MATERIALS AND METHODS

Cortical Circumferential Profile

Harris et al. (15) described the generation of a cortical circumferential profile (CCP) for studying patterns of cortical perfusion in SPECT images. They highlight the difficulties associated with manual placement of multiple regions of interest (ROI) over a continuous structure such as the cortex, noting the time-consuming nature of such a task in particular. The CCP is obtained from a given SPECT image slice in several stages:

1. The outer edge of the cortex is defined by an operator with reference to the grey scale image, as is a marker defining the best estimate of the point of intersection of the cortical edge with the anterior inter-hemispheric midline (to allow normalization for rotational offset).
2. The geometric center of this outer boundary is determined, from which are drawn a series of radii with 6° separation, such that they intersect with the cortical edge at 60 locations. The radii are rotated so that the hemispheric midline marker lies directly between two adjacent radii.
3. Sixty points are defined, each lying along one of the radii at a distance of 1 cm from the brain edge in the direction of the center. These points are used as the centers of a series of 1-cm^2 areas.
4. The average count rate in each area is determined and normalized to the mean cerebellar count. The normalized mean count rates for each area, plotted against the radial angle, define the CCP. Note that the CCP always consists of a vector of 60 numbers and thus normalizes for overall brain size.

Harris et al. claim that the CCP is more reliable, objective and easier to produce than alternatives based on operator-defined ROIs. They substantiate these claims by generating CCPs for 23 subjects, 15 of whom had been diagnosed as having probable Alzheimer's disease (16), the remainder being age-matched normals. For each subject, CCPs were generated, blind to diagnosis, using two axial slices: the first slice (BG) was that which "best passed through the basal ganglia" according to a visual inspection; the second slice (SU) was 1.1 cm superior to the first. The reliability of the CCP method compared favorably with that of a method requiring the manual placement of ROIs and analysis of the mean CCPs obtained from patients and normals indicated significant differences. The principal finding was of significant hypoperfusion in the temporo-parietal regions of patients relative to normals.

Further compression of the profile information was achieved by taking average count values over six contiguous values within the CCP; each resulting value thus represented the mean perfusion value over a 36° cortical arc, with five such values per hemisphere. The regions from which these values are extracted are chosen to approximate functional zones within the cortex, namely frontal (FR), posterior-frontal (PF), sensory-motor (SM), temporo-parietal (TP) and occipital (OC) zones. Pearlson et al. (18) used such

Received Aug. 25, 1994; revision accepted Jun. 17, 1995.

For correspondence or reprints contact: Michael P.A. Page, PhD, M.R.C. Applied Psychology Unit, 15, Chaucer Rd., Cambridge, CB2 2EF, United Kingdom.

compressed zonal profiles in a study which employed traditional statistical techniques to discriminate between scans from Alzheimer's disease and control subjects.

The first task involved application of the CCP method to a new and larger corpus of SPECT scans than that used by Harris et al. The results are compared with those described above.

Data Collection and Analysis

Subjects. There were 31 right-handed patients (17 men) selected from consecutive referrals to the Memory Clinic at the Maudsley Hospital, all of whom fulfilled the NINCDS/ADRDA criteria for probable Alzheimer's disease (16). Each patient underwent a standardized assessment procedure which included history, physical and mental state examination, blood tests and CT. Alzheimer's disease patients had a mean age of 67.9 yr (s.d. 7.7 yr, range 53–83 yr) and a mean score on the Mini-Mental State Examination (MMSE) of 17.1 (s.d. 5.1).

We also studied 26 right-handed, age-matched controls (10 men), mainly recruited from the spouses of the chosen patients. The mean age of the normal group was 64.1 (s.d. 9.0, range 48–85) and their mean MMSE score was 28.8 (s.d. 1.0). None of the controls had any symptoms or signs of dementia.

All subjects were drug-free for at least 3 wk, both at the time of scanning and of neuropsychological assessment.

The SPECT images from this group have already been subjected to conventional methods of image analysis (13). In this earlier report, regional cerebral blood flow was assessed both semiquantitatively and from measurements from 18 cortical and 4 subcortical ROIs, normalized to the mean cerebellar flow. Alzheimer's disease patients were shown to have foci of reduced flow in the temporal, parietal, frontal and left occipital areas.

Imaging and Image-Processing Procedures

Imaging was performed using a ^{99m}Tc -labeled hexa-methyl propylene amine oxime (HMPAO) tracer and a scanner linked to a computer. Subjects received an intravenous injection of 550 MBq ^{99m}Tc -HMPAO under resting conditions with eyes closed in a quiet room. Imaging was performed within 90 min of tracer administration, producing 14 overlapping transverse slices parallel to the orbito-meatal line. Each slice, acquired over 3 min, was 15 mm thick with an in-plane resolution of 7.5 mm.

For each subject, two slices were selected by expert visual inspection: the first was that slice that best passed through the basal ganglia (BG); the second, that which best passed through the cerebellum. The slices were displayed and manipulated within the MIDAS system developed by Peter Freeborough at Imperial College. CCP generation involved the definition of a single ROI on each slice: the operator made a visual assessment of the location of the cortical edge and defined it on the BG slice by clicking a mouse at multiple points; the boundary of the cerebellum was defined in a similar way on the second slice. In addition, the interhemispherical marker was defined by a single mouse click. All subsequent steps in the generation of the CCP were automatic: these comprise the calculation of the mean cerebellar perfusion value, the definition of the 60 cortical sample areas and the generation of the profile itself. All CCPs were generated blind to clinical diagnosis.

RESULTS

For each group of subjects, a mean profile was produced as previously reported (15). The reliability of these mean profiles was assessed by having the same operator generate each profile twice, on separate days. Intraoperator reliability was expressed by correlation coefficients for all 60 profile points: all correlations were greater than 0.89, apart from five values taken from regions near the interhemispherical line, which were in the range of 0.85–0.89. This supported the operator's subjective belief

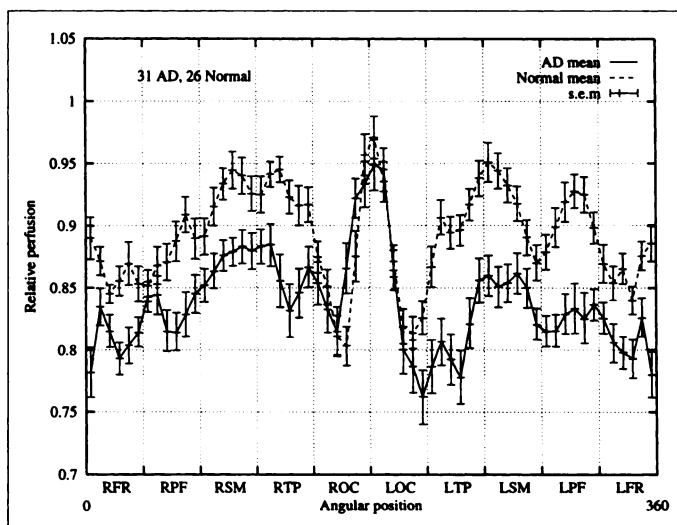


FIGURE 1. Mean profiles for each group from first blind profile generation.

that the cortical edge was often a little more difficult to define in these regions. For the compressed zonal profiles, correlation coefficients for all 10 regions were greater than 0.95. Figure 1 shows the mean profiles for the 31 Alzheimer's disease patients and the 26 controls from the first profile generation: the x-axis represents angular position and is additionally labeled with the corresponding zones (e.g., RTP = right temporo-parietal), the y-axis represents mean perfusion value relative to that of the cerebellum and the error bars denote the s.e.m.

Figure 2 shows the differences between the means for the two groups (controls minus patients) at each angular position and for each of two profile generations—the greatest deficits for patients relative to controls are found in the left and right temporo-parietal regions and the left posterior frontal regions. In addition, the two sample points on either side of the anterior interhemispherical midline show large deficits, although these are not sustained to the same degree across the whole frontal region.

Unlike the results obtained by Harris et al. (15), the mean Alzheimer's disease profile is not below the mean normal profile at all angular positions; in the vicinity of the posterior interhemispherical midline, the Alzheimer's disease mean profile goes above the mean control profile. This unexpected increased

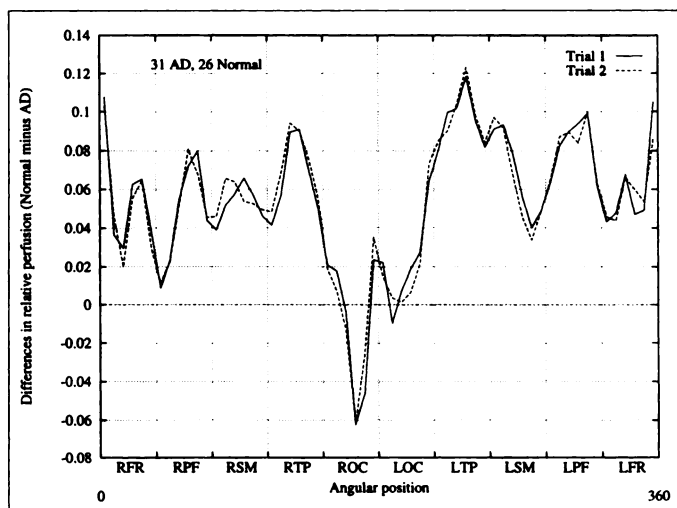


FIGURE 2. Differences between mean profiles for two blind profile generations.

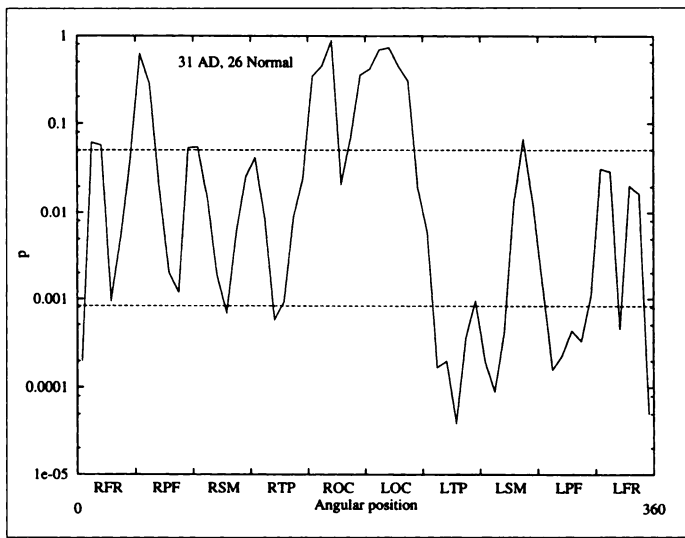


FIGURE 3. Significance profile for differences between group mean profiles.

regional flow for Alzheimer's disease patients over controls was not, however, statistically significant.

Figure 3 shows a "significance profile," which plots the p value obtained from a two-tailed t-test at each angular position. The upper dashed line corresponds to $p = 0.05$, indicating significance without the Bonferroni correction; the lower dashed line corresponds to $p = 0.00083(0.05/60)$, indicating significance with the Bonferroni correction. This correction assumes uncorrelated data, an assumption that is probably not justified here; to the extent that the data are correlated, our correction make conservative estimates of statistical significance. As shown by Harris et al. (15), the samples from the left temporo-parietal region (LTP) show the most significant differences between the two groups.

Further statistical analysis was performed on the compressed zonal profiles. Mean compressed profiles for patients and controls are shown in Figure 4 and the difference between the two (control minus patient) is shown in Figure 5. A significance profile for the group-mean differences is plotted in Figure 6.

Eight of the ten regions show differences significant at the $p = 0.05$ level, and seven of these show significant differences even after application of the Bonferroni correction ($p < 0.005$). For the regional averages, the LPF and LTP regions show the most significant differences between the two groups. The LTP

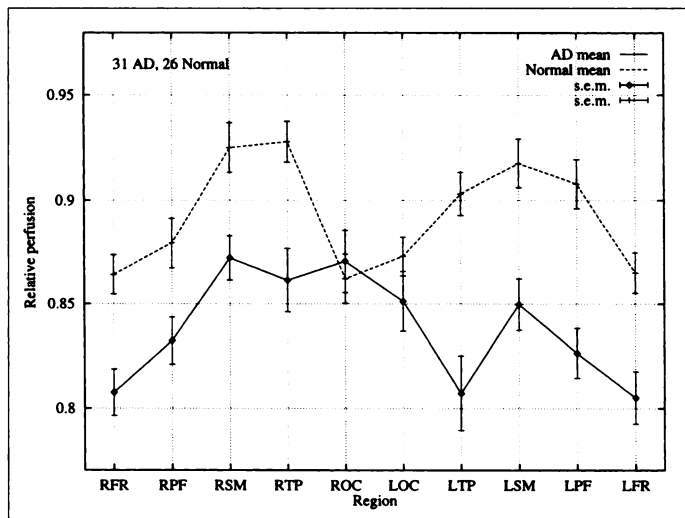


FIGURE 4. Mean compressed profiles for each group from the first blind profile generation.

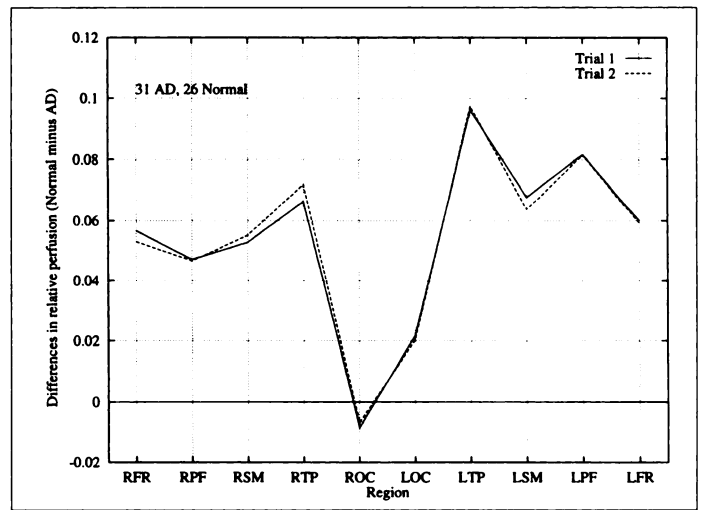


FIGURE 5. Differences between compressed mean profiles for two blind profile generations.

result is consistent with that of Harris et al. (15), but the LPF result differs for the two studies.

DISCUSSION

Comparison of these results with those of Harris et al. (15) shows that while the mean profiles for each group in Harris et al. are more clearly separated, the increased statistical power that results from our use of a much larger subject group, reveals significant differences between patients and controls in a larger number of cortical areas. Analysis of the compressed zonal profiles suggests that only the occipital areas are unaffected by Alzheimer's disease. Both studies show high statistically significant differences in the left temporo-parietal region, while our study indicates comparable differences in the left posterior-frontal region. This evidence of frontal involvement is supported by O'Brien et al. (13), who used manually-defined ROIs to investigate perfusion patterns in the current group of patients.

Data Classification

Our next task was to investigate whether the profile information generated above could be used in automated diagnosis. The profiles were analyzed by being subjected to a number of traditional statistical techniques and used to train a neural-network classifier. For comparison, performance was assessed relative to that of an expert viewer. All performance results

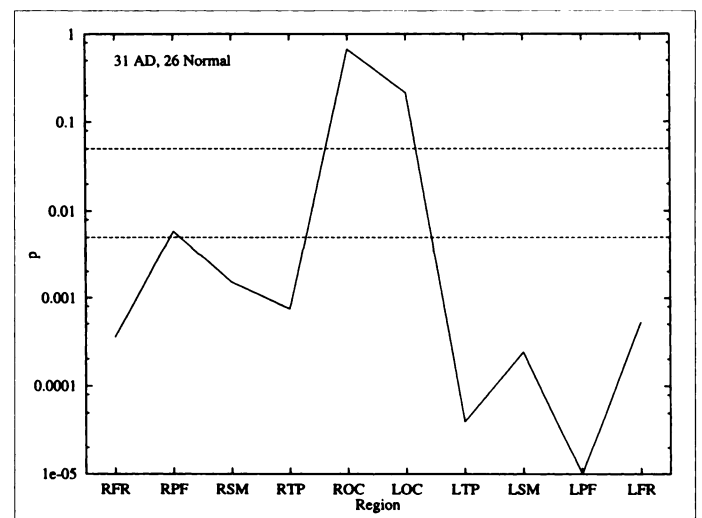


FIGURE 6. Significance profile for differences between group mean compressed profiles.

were reported on the basis of the relative operating characteristic (ROC) curve (17). One generates an ROC curve by plotting the true-positive response ratio against the false-positive response ratio for various settings of a decision criterion. The area under the resulting curve gives a single measure of diagnostic performance that is “uninfluenced by decision biases and prior probabilities” (17). This measure can alternatively be derived from the intercept and slope values obtained by plotting the ROC curve on a binormal graph (17), and this was the method preferred here.

Statistical Analyses

Before the application of any of the statistical techniques, the compressed zonal profiles obtained above were normalized. This was done purely to expedite later processing and consisted of scaling the profile values so that they all lay in the interval [0,1], which indicates the standard mathematical notation for the range 0–1 inclusive. The normalization was performed across the whole set, rather than separately for each profile, thus ensuring that the structure of the data was unaffected.

The first statistical analysis performed on the compressed CCP data was the same as that detailed by Pearlson et al. (18). The ability of a perfusion measure, taken from a single region of the compressed profile, to allow discrimination between patients and controls was determined by the placement of a discriminant function line (see below). By varying the position of the discriminant function line (DFL), we can generate an ROC curve and assess performance.

The second statistical technique involved the training of a discriminant analysis classifier (DAC). Kippenhan et al. (19,20) used this type of classifier in the evaluation of a neural-network classifier (NNC) applied to perfusion profiles extracted from PET scans. In the former paper, the profiles consisted of eight-dimensional vectors representing mean metabolism in each of eight lobar regions; in the latter paper, 25-dimensional vectors representing mean metabolism in 25 lobules were additionally employed. The use of the same statistical technique facilitates comparison with the results presented in these papers, but caution must still be exercised. Discriminant analysis, using optimal quadratic discriminants, was carried out using the SAS statistical package (21). ROC curves were generated by varying the prior probabilities for class membership. Kippenhan et al. (19,20) used larger datasets than the one used here and assessed the *cross-validation* performance of both of their classifiers (discriminant analysis and neural network) by dividing the dataset into two independent groups: a training set and a test set. For the simulations presented here, we used the L-method of cross-validation testing: for *each pattern* in the complete dataset, a classifier is trained on all *other* patterns and then tested with the pattern itself. Use of the L-method maximizes the size of the training set while preserving the independence of the test set. Ideally, one would want to further test the trained classifier on an entirely new set, but this was not feasible with the numbers of subjects available.

Neural Network Classifier

The structure of a neural network suited to the classification task is shown in Figure 7. The three-layer feedforward network has 10 input units, one for each element of the compressed zonal profiles, a number of so-called hidden units that are optimized for the task in hand (see below) and a single output unit. Successive layers in the network are fully connected by a matrix of adaptable weighted connections. In addition, a tonically active “bias” unit sends input via weighted connections to each unit in the hidden and output layers. Briefly, training is performed as follows: each profile in the training set is

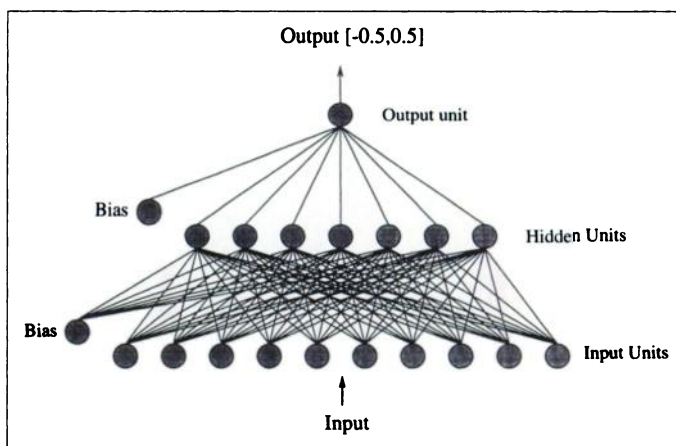


FIGURE 7. Three-layer feedforward neural network.

presented at the input of the network, and activation is fed forward through the network; the resulting output value is compared with a desired value which indicates the class membership of the current input. In this case, a desired output of -0.5 indicated that the current input was an Alzheimer’s disease patient and a desired output of $+0.5$ indicated a normal subject. The error, i.e., the desired output minus the actual input, is then “propagated” back through the network and the connection weights at each stage are changed so as to reduce the error on subsequent presentation of the same input. Testing is accomplished by presenting test patterns to the learned network giving a diagnostic output value in the range $[-0.5, 0.5]$. We used Fahlman’s Quickprop algorithm, a variation of the standard backpropagation learning rule which can greatly improve convergence times (22). The performance of the neural network classifier can be optimized with reference to the number of hidden units and the number of training “epochs” (23). Too much training can lead to overfitting, adversely affecting the network’s capacity to generalize in response to novel input. Optimum performance was assessed by testing networks with even numbers of hidden units in the range 4–20, at all 500-epoch increments up to 10,000 epochs. The results presented refer to the combination which gave the best performance averaged over five trials, each trial using random initial weights and a random ordering of the input set. The ROC measure itself was obtained by varying an output decision threshold.

Expert Viewer Classification

To gauge the usefulness of the automated classification methods, two experts were asked to examine the SPECT scans and to rate them for perceived evidence of Alzheimer’s disease. The viewer was informed of the two group diagnoses but was blind to individual clinical diagnosis during rating. A five-point rating scale was used where 1 = definitely not Alzheimer’s disease, 2 = probably not Alzheimer’s disease, 3 = borderline Alzheimer’s disease, 4 = probable Alzheimer’s disease and 5 = definite Alzheimer’s disease. The experts viewed all the image slices for a given subject, each slice consisting of 128×128 pixels; slices could be enlarged to 256×256 pixels to aid more detailed inspection. Viewing was performed on separate days under two conditions. In Condition 1, a grey scale was used so that perfusion data in the separate slices of a given brain image were displayed so that the pixel corresponding to the point of highest perfusion in the whole-brain image appeared white (grey level = 255) and all other pixels in that brain image were scaled accordingly, thereby allowing comparison of perfusion levels between slices. In addition, a lower perfusion

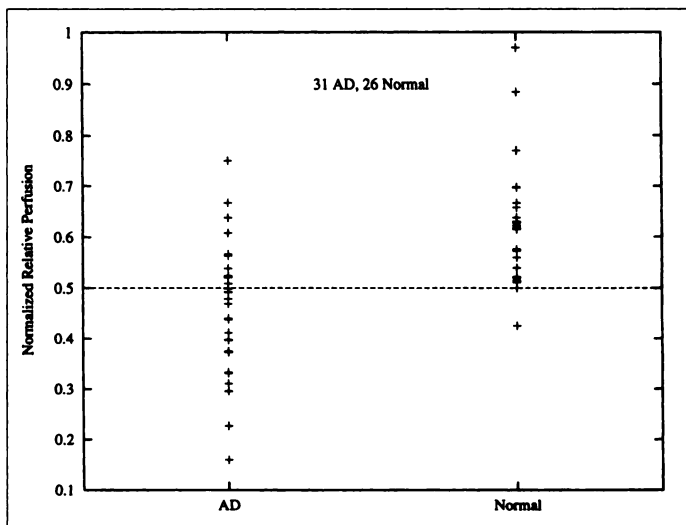


FIGURE 8. Scatterplot for LPF perfusion scores.

threshold, below which activities were displayed as black, could be varied by the viewer as desired. In Condition 2, a color map that had been specifically designed to view brain SPECT images by one of the experts was used; the strategic placing of prominent color boundaries permitted semiquantitative viewing. Finally, for each brain image, attention was drawn to the BG image slice used to generate the CCP. The results reported are those of the better of the two experts (the same expert in each condition).

RESULTS

Discriminant Function Line

A preliminary stepwise discriminant-function analysis identified the LPF as the region that best supported between-group discrimination. For the LPF perfusion score, the best DFL led to 78.9% correct classification and an ROC performance of 0.850. Figure 8 shows a scatterplot for the normalized LPF perfusion score for each subject group, together with the optimal discriminant function line.

Pearlson et al. (18) were able to achieve 89% correct classification using this simple technique, but the numbers of patients and normals (20 and 8, respectively) were much smaller than those employed here.

Discriminant Analysis Classifier

The discriminant analysis classifier (DAC) gave an ROC area of 0.821, with a maximum of 77.2% correct classification. For comparison, Kippenhan et al. (19) report a maximum DAC performance of 0.80 using nonzero-mean versions of their eight-dimensional input patterns, whereas in another study, Kippenhan et al. (20) report equivalent values of 0.86 for lobar profiles and 0.95 for lobular profiles, both derived from high-resolution PET data.

Neural Network Classifier

The optimized neural network gave a mean ROC performance across five trials of 0.913 (s.d., 0.015), and a maximum classification rate of 88.1% correct (s.d., 2.9), using a small negative threshold. The optimum network used 16 hidden units and was trained for 4500 epochs. While this number of hidden units might seem excessive, Weigend (24) has pointed out that given the size of the training set, large networks stopped early in training can often perform better generalization than small networks trained for longer time periods. Again for comparison, the network used by Kippenhan et al. (19) gave an ROC performance of 0.85; the networks used in their other study (20)

TABLE 1
Summary of Classification Results

Classifier	ROC area	Max. % Correct
DFL-LTP	0.776	75.4
DFL-LPF	0.850	78.9
DAC	0.821	77.2
NNC	0.913	88.1
Expert (Cond. 1)	0.768	73.7
Expert (Cond. 2)	0.792	73.7

gave the best ROC performance values of 0.87 for the lower resolution PET data and 0.95 for higher resolution data, both achieved using 25-dimensional lobular profiles.

Expert Viewer

Under Condition 1 (grey scale), the expert viewer achieved an ROC performance of 0.768, with a maximum classification rate of 73.7%. Viewing under Condition 2 showed an improvement; the ROC performance rose to 0.823, while the maximum percentage correct remained at 73.7%. The expert viewer used by Kippenhan et al. (19) achieved an ROC performance of 0.89; we will not attempt to account for the disparity in expert performance between the two studies.

These results are summarized in Table 1 and the corresponding ROC curves are plotted in Figure 9. The curves shown are best fit curves generated from the intercept and slope information derived from the bivariate normal plots.

DISCUSSION

Our results permit two conclusions: First, given this particular input pattern set, the neural network performs the classification task better than other statistical methods. Second, the neural network performs better than the expert viewers. The latter comparison is qualitatively different from the former; in the case of the comparison with other statistical techniques, the information used is the same for each method. By contrast, the expert viewer, in making a diagnosis, draws on experience from outside the current input set. Additionally, the expert viewer can visualize all the slices in a given brain image, rather than being given the "restricted view" afforded to the automated methods. Interestingly, of the seven profiles which are consistently misclassified by the NNC, only one was also misclassified by the expert viewer, whereas four were also misclassified by the DFL and the DAC. This might indicate that the expert viewer

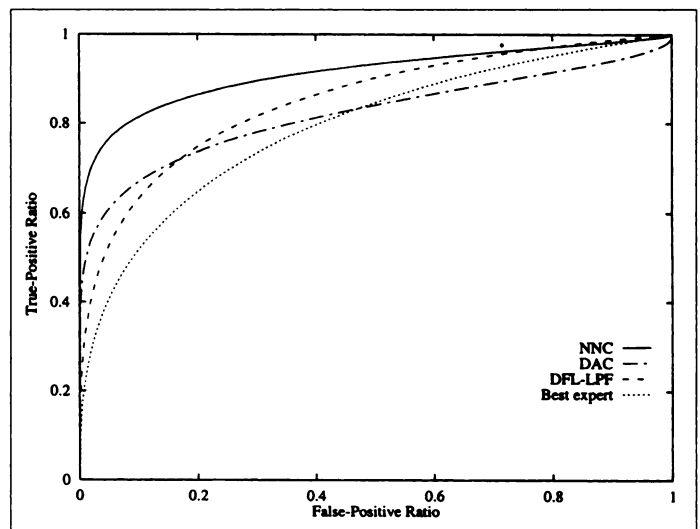


FIGURE 9. ROC curves for various classification methods.

was not, for whatever reason, focussing on those brain areas which underpin the ability of the profiling technique to support between-group discrimination.

The comparison with the results of Kippenhan et al. (19,20) shows that the compressed cortical circumferential profiles, generated from SPECT brain scans, enable better discrimination between patients and normals than do any of the profiles derived from their lower resolution PET data or the eight-dimensional lobar profiles derived from the higher resolution data. We must, of course, be cautious in making too much of the comparison, since the subject groups were entirely separate, Kippenhan et al. used a larger group (41 patients, 50 controls), where the patients had a mean MMSE score of 15.0 (s.d. 7.3). Nonetheless, the fact that our method using SPECT data offers performance comparable with those applied to PET data is encouraging and perhaps highlights the merits of the CCP as a profiling technique. Moreover, the generation of a CCP is largely automated, requiring the manual definition of only two ROIs. The lobar/lobular profiles used by Kippenhan et al. (19,20) were generated from 67 ROIs, the definition of which require considerable operator intervention.

CONCLUSION

We have shown how the CCP technique introduced by Harris et al. (15) is useful in illustrating the different patterns of cortical perfusion found in Alzheimer's disease patients relative to age-matched controls. The familiar pattern of temporoparietal and frontal deficits emerges. The profiling procedure is simple, requires relatively little operator intervention and produces profiles of a constant dimensionality. These profiles are well suited to automated classification, and we have shown how a variety of classifiers perform in a task requiring discrimination of profiles from Alzheimer's disease patients and controls. Most of the classifiers outperform the expert viewers; the neural network does so by a considerable margin. They also outperform the equivalent classifiers used by Kippenhan et al. (19) but not the best of those used by Kippenhan et al. (20).

Further work will involve applying the methods described here to larger datasets, including PET data. A particular benefit of the CCP technique is that the provenance, and even modality, of a given brain image is largely irrelevant. It is hoped that this work will ultimately lead to a diagnostic tool suitable to assist routine clinical practice.

ACKNOWLEDGMENTS

We thank Prof. Richard Kitney, Dr. Keith Straughan and Dr. Anil Bharath of the Sir Leon Bagrit Center for Biomedical Systems, Imperial College, London for their support; Dr. John Barrett for acting as an expert viewer; Peter Freeborough for the development of the MIDAS system; Prof. Igor Aleksander for initial discussions and arranging contacts at Imperial College; and the remaining authors of O'Brien et al. (13), namely Drs.

Sarah Egger, Ghulam Syed, Barbara Sahakian and Prof. Raymond Levy, for allowing the use of scan data from their earlier study. We thank two anonymous reviewers for their comments on an earlier draft. Supported by grant G9200915N from the United Kingdom Medical Research Council.

REFERENCES

1. Miller AS, Blott BH, Hames TK. Review of neural network applications in medical imaging and signal processing. *Med Biol Eng Comput* 1992;30:449-464.
2. Stubbs DF. Multiple neural network approaches to clinical expert systems. *SPIE Appl Artif Neural Networks* 1990;1294:433-441.
3. Wu Y, Giger ML, Doi K, Vyborny CJ, Schmidt RA, Metz CE. Artificial neural networks in mammography: application to decision making in the diagnosis of breast cancer. *Radiology* 1993;187:81-87.
4. Agyei-Mensah SO, Lin FC. Application of neural networks in medical diagnosis: the case of sexually-transmitted diseases. *Australas Phys Eng Sci Med* 1992;15:186-192.
5. Lo SC, Freedman MT, Lin JS, Mun SK. Automatic lung nodule detection using profile matching and back-propagation neural network techniques. *J Digit Imaging* 1993;6:48-54.
6. Scott JA, Palmer EL. Neural network analysis of ventilation-perfusion lung scans. *Radiology* 1993;186:661-664.
7. Boone JM, Gross GW, Greco-Hunt V. Neural networks in radiological diagnosis: I. Introduction and illustration. *Invest Radiol* 1990;25:1012-1016.
8. Gross GW, Boone JM, Greco-Hunt V, Greenberg B. Neural networks in radiological diagnosis: II. Interpretation of neonatal chest radiographs. *Invest Radiol* 1990;25:1017-1023.
9. Aston ML, Wilding P. Application of neural networks to the interpretation of laboratory data in cancer diagnosis. *Clin Chem* 1992;38:34-38.
10. Hellman RS, Tifofsky RS, Collier BD, et al. Alzheimer disease: quantitative analysis of I-123-iodoamphetamine SPECT brain imaging. *Radiology* 1989;172:183-188.
11. Holman BL, Johnson KA, Gerada B, Carvalho PA, Satlin A. The scintigraphic appearance of Alzheimer's disease: a prospective study using technetium-99m-HMPAO SPECT. *J Nucl Med* 1992;33:181-185.
12. Johnson KA, Holman BL, Rosen TJ, Nagel JS, English RJ, Growdon JH. Iodine-123-iodofetamine SPECT is accurate in the diagnosis of Alzheimer's disease. *Arch Intern Med* 1990;150:752-756.
13. O'Brien JT, Egger S, Syed GMS, Sahakian BJ, Levy RA. Study of regional cerebral blood flow and cognitive performance in Alzheimer's disease. *J Neurol Neurosurg Psychiatry* 1992;55:1182-1187.
14. Launes J, Sulkava R, Erkinjuntti T, et al. Technetium-99m-HMPAO SPECT in suspected dementia. *Nucl Med Commun* 1991;12:757-765.
15. Harris GJ, Links JM, Pearson GD, Camargo EE. Cortical circumferential profile of SPECT cerebral perfusion in Alzheimer's disease. *Psychiatry Res* 1991;40:167-180.
16. Mc Khann G, Drachman D, Folstein M, Katzman R, Price D, Stadlan E. Clinical diagnosis of Alzheimer's disease: report of the NINCDS-ADRDA Work Group under the Dept. of Health and Human Task Force in Alzheimer's Disease. *Neurology* 1984;34:939-944.
17. Swets JA. Measuring the accuracy of diagnostic systems. *Science* 1988;240:1285-1293.
18. Pearson GD, Harris GJ, Powers RE, et al. Quantitative changes in mesial temporal volume, regional cerebral blood flow, and cognition in Alzheimer's disease. *Arch Gen Psychiatry* 1992;49:402-408.
19. Kippenhan JS, Barker WW, Pascal S, Nagel J, Duara R. Evaluation of a neural-network classifier for PET scans of normal and Alzheimer's disease subjects. *J Nucl Med* 1992;33:1459-1467.
20. Kippenhan JS, Barker WW, Nagel J, Grady C, Duara R. Neural-network classification of normal and Alzheimer's disease subjects using high-resolution and low-resolution PET cameras. *J Nucl Med* 1994;35:7-15.
21. *SAS/STAT Guide for Personal Computers*, version 6 edition. Cary, NC: SAS Institute Inc.
22. Fahlman SE. Faster-learning variations on back-propagation: an empirical study. In: Touretzky DS, ed. *Advances in neural information processing systems 2*. Los Altos, CA: Morgan Kaufmann Publishers, 1988:38-51.
23. Kippenhan JS, Nagel JH. Optimization and evaluation of a neural-network classifier for PET scans of memory-disorder subjects. *Proc 13th Ann Int Conf IEEE/EMBS* 1991;13:1472-1473.
24. Weigend AS. On overfitting and the effective number of hidden units. In: *Proceedings of 1993 Connectionist Models Summer School*. Hillsdale, NJ: Lawrence Erlbaum, 1994:335-342.